JOURNAL OF GEOPHYSICAL RESEARCH, VOL. 112, F03S22, doi:10.1029/2006JF000596, 2007

Analysis of glacial earthquakes

Victor C. Tsai[1] and Göran Ekström[1]

Received 12 June 2006; revised 27 October 2006; accepted 22 November 2006; published 14 April 2007.

[1] In 2003, Ekström et al. reported on the detection of a new class of earthquakes that occur in glaciated regions, with the vast majority being in Greenland. The events have a characteristic radiation pattern and lack the high-frequency content typical of tectonic earthquakes. It was proposed that the events correspond to large and sudden sliding motion of glaciers. Here we present an analysis of all 184 such events detected in Greenland between 1993 and 2005. Fitting the teleseismic long-period surface waves to a landslide model of the source, we obtain improved locations, timing, force amplitudes, and force directions. After relocation, the events cluster into seven regions, all of which correspond to regions of very high ice flow and most of which are named outlet glaciers. These regions are Daugaard Jensen Glacier, Kangerdlugssuaq Glacier, Helheim Glacier, the southeast Greenland glaciers, the northwest Greenland glaciers, Rinks Isbrae, and Jakobshavn Isbrae. Event amplitudes range from 0.1 to 2.0 $\times$ 10^{14} kg m. Force directions are consistent with sliding in the direction of glacial flow over a period of about 50 s. Each region has a different temporal distribution of events. All glaciers are more productive in the summer, but have their peak activity in different months. Over the study period, Kangerdlugssuaq has had a constant number of events each year, whereas Jakobshavn had most events in 1998–1999, and the number of events in Helheim and the northwest Greenland glaciers has increased substantially between 1993 and 2005. The size distribution of events in Kangerdlugssuaq is peaked above the detection threshold, suggesting that glacial earthquakes have a characteristic size.

Citation: Tsai, V. C., and G. Ekström (2007), Analysis of glacial earthquakes, *J. Geophys. Res.*, *112*, F03S22, doi:10.1029/2006JF000596.

1. Introduction

[2] Since the 1980s, glaciologists have known that both the Greenland and Antarctic ice sheets are drained by narrow but fast moving features known as ice streams and outlet glaciers [*Bauer*, 1961; *Morgan et al.*, 1982]. More recently, it has been observed that these features display a wide range of time-varying behavior with timescales ranging from thousands of years down to a few minutes [e.g., *Alley and Whillans*, 1991; *Bindschadler et al.*, 2003; *Howat et al.*, 2005]. Although a great deal of work has been done to understand what controls these variations in ice velocity, many aspects of glacial dynamics are still poorly understood [e.g., *Paterson*, 2002; *Hooke*, 2005].

[3] In 2003, *Ekström et al.* [2003] presented evidence for the detection of a new class of earthquakes associated with ice motion. Although seismic studies of glacial regions have described a wide range of phenomena [e.g., *Van Wormer and Berg*, 1973; *Weaver and Malone*, 1979; *Wolf and Davies*, 1986; *Qamar*, 1988; *Deichmann et al.*, 2000; *Stuart et al.*, 2005], all seismic studies prior to that by *Ekström et al.* [2003] describe earthquakes with magnitudes smaller than 2.8 and with dominant periods less than 1 s. In contrast, *Ekström et al.* [2003] describe earthquakes with dominant periods between 35 and 150 s and surface wave magnitudes between 4.6 and 5.1, thus describing a new glacial phenomenon. The majority of these "glacial earthquakes" occur in Greenland and are characterized by their lack of high-frequency radiation compared to that of standard earthquakes of similar magnitudes. *Ekström et al.* [2003] further observe that the radiation patterns of the events are inconsistent with the standard earthquake faulting mechanism but are much better described by a "landslide" model thus leading them to interpret the events as sudden, rapid movement of ice. *Ekström et al.* [2003, 2006] also observe a seasonal variation in the event distribution, with fewer events in the winter months, leading them to speculate that meltwater may play an important role in the occurrence of glacial earthquakes.

[4] The earthquake detection algorithm as described by *Ekström* [2006] has now been used on all the available global seismic data from 1993 to 2005. This analysis has resulted in the detection of 184 glacial earthquakes in Greenland. Here, we present a detailed seismic analysis of these 184 events. We obtain improved estimates of the locations of the events compared with those of *Ekström et al.* [2006]. We also obtain estimates of the amplitude and direction of the force associated with each event, something that has not previously been done systematically for glacial

[1]Department of Earth and Planetary Sciences, Harvard University, Cambridge, Massachusetts, USA.

0148-0227/07/2006JF000596$09.00

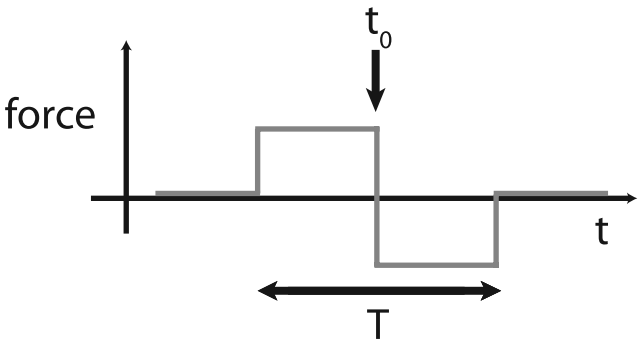

Figure 1. Schematic of the symmetric boxcar forcing function used for waveform inversion. T is the full duration of the event and is taken to be 50 s in all inversions; t_0 is the centroid time of the event.

earthquakes. These new source parameters allow us to draw a close association between glacial earthquakes and fast flowing features (ice streams and large outlet glaciers) of the Greenland Ice Sheet. We are further able to suggest some relationships between some glacial earthquake parameters and certain glaciological parameters. However, given the lack of constraints on many key glaciological parameters, it would be premature to make conclusive statements about the glacial physics involved. Further observation and research are required to make such statements.

2. Analysis

[5] We analyze 184 Greenland events that result from the application of the earthquake detection algorithm of *Ekström* [2006]. From the initial detections, we have estimates of the origin time, epicenter, and a long-period surface wave magnitude (M_{SW}) of the events. The detection origin times are accurate to within approximately 10 s, locations accurate to within a few hundred km, and M_{SW} accurate to within 0.1–0.2 magnitude units. As will be shown, the analysis presented here significantly decreases all of these uncertainties. The range of M_{SW} for the glacial events is 4.6–5.1, where M_{SW} = 4.6 corresponds to the lowest-magnitude earthquake that can be detected with the current detection algorithm.

[6] We use seismic data recorded by the IRIS Global Seismographic Network (GSN), filtered in the 35–75 s, 40–100 s, or 50–150 s period band, depending on which period band has a better signal-to-noise ratio for each event. Since the signal-to-noise ratio is often small, we only use between 10 and 40 of well-distributed, high signal-to-noise stations in the analysis of each event. Vertical, transverse, and longitudinal component seismograms are all used when appropriate. Fewer stations are typically used for smaller events.

[7] Similar to *Ekström et al.* [2003], we find that the standard centroid moment tensor (CMT) description [*Dziewonski et al.*, 1981] of earthquakes provides poor fits to the glacial earthquake surface wave waveforms. Since the CMT description utilizes a six-component moment tensor, it can represent the double-couple faulting on a plane that characterizes standard earthquakes as well as a more general source, including an isotropic explosion or a dipole-like source. For these inversions, the modeled waveforms fit the data waveforms with residual variance (normalized misfit) typically between 0.6 and 0.7.

[8] *Ekström et al.* [2003] show that modeling the glacial earthquakes with the centroid single force (CSF) model of *Kawakatsu* [1989], which has been used to model landslide events successfully [*Kanamori and Given*, 1982; *Brodsky et al.*, 2003], yields more satisfactory fits to the data. The CSF model can be used to represent a mass that slides down a slope with an acceleration and then deceleration phase. As the mass accelerates, a force is exerted on the Earth in the direction opposite to the mass acceleration, thus creating seismic waves. In the simplest formulation, there is constant acceleration followed by constant deceleration of equal and opposite amplitudes, yielding a symmetric boxcar forcing function as depicted in Figure 1. We use the symmetric CSF as a first approximation to the actual forcing function to perform waveform inversions. As in the standard CMT inversions [*Dziewonski et al.*, 1981], the problem is nonlinear and the best fit solution is obtained by iterative inversion.

[9] Under the symmetric boxcar CSF formulation, each inversion has 4 free parameters in addition to the centroid time and location of the event: the amplitudes for the 3 components of the force and the duration. All events are well fit with source duration set equal to 50 s, consistent with the fact that waves excited by such a source have their dominant period close to 50 s and the events were detected using data in the 35–150 s period band. The modeled seismograms are not very sensitive to changes in duration on the order of 10 s, with such changes causing residual variance to vary by between 0.01 and 0.05. Such changes of duration also cause substantial differences in retrieved force amplitude, with longer durations resulting in increased amplitudes of up to 50% and shorter durations resulting in decreased amplitudes of up to 30%. In this analysis, we set the duration of all CSFs to 50 s and all reported amplitudes are with this assumption for the duration. Since it is likely that larger events have longer durations than smaller events, the actual range of amplitudes is possibly a factor of two larger than the range we present.

[10] The amplitude of the CSF (which is a twice-time-integrated force), A, has one possible simple interpretation in terms of the simple symmetric boxcar force model [*Kawakatsu*, 1989]:

$$A = D \cdot M \tag{1}$$

where M is the mass of the slider block (SB) and D is the distance traveled by the SB. The CSF amplitudes we report will be in this "mass times distance" form. Other physical parameters can also be expressed in terms of A. The maximum velocity change of the SB is given by

$$\Delta V = 2A/(M \cdot T) \tag{2}$$

where T is the duration of the event. Describing the resistive force, F, in terms of an average coefficient of friction, f, then

$$F = f \cos\theta \cdot Mg \tag{3}$$

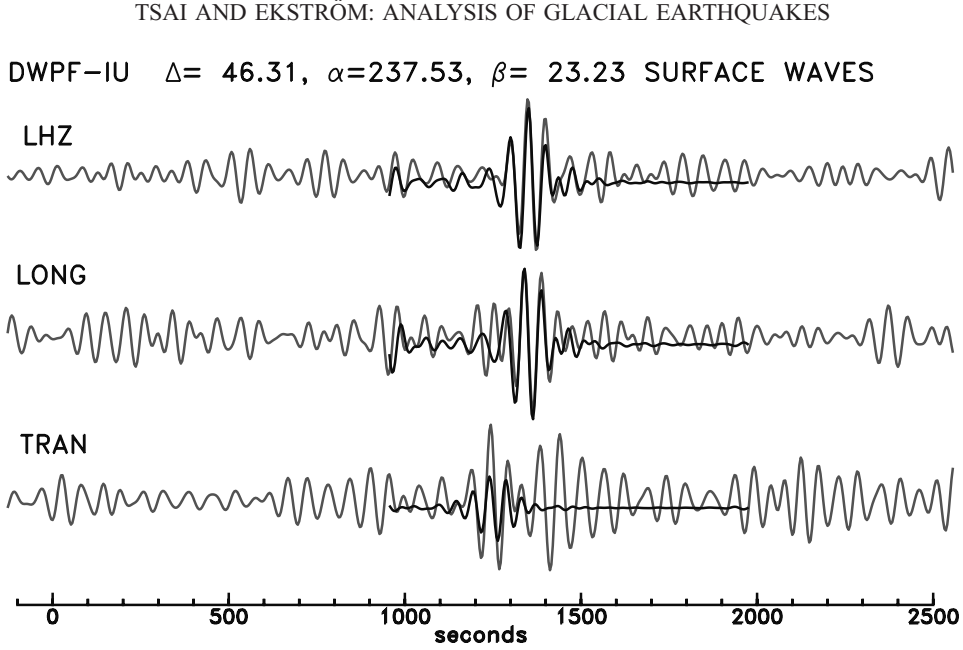

Figure 2. Sample seismograms for the 7 February 2001 event recorded at station DWPF (28.11°N, −81.43°E). Gray lines show data seismograms; black lines show synthetic seismograms, offset slightly vertically for clarity. Δ is the distance (in degrees) of the station from the earthquake, α is the azimuth of the station relative to the earthquake, and β is the azimuth of the earthquake relative to the station. The zero time is as in Table 1. The period range is 35–75 s. LHZ, vertical; LONG, longitudinal; TRAN, transverse.

where g is the gravitational acceleration and θ is the slope angle. The difference between F during an event and steady state is

$$\Delta F = 4A/T^2 \tag{4}$$

and the change in f is ($\theta \ll 1$ so $\cos\theta \sim 1$)

$$\Delta f = 4A/\left(Mg \cdot T^2\right) \tag{5}$$

Waveform inversions using the symmetric CSF model result in modeled seismograms that fit the data well, with residual variance of the best fit inversion typically between 0.3 and 0.5. This observed improvement in residual variance compared with CMT modeling (residual variance of 0.6–0.7) is the reason we use the CSF formulation. The events generally have a two-lobed radiation pattern, with maxima perpendicular to sliding for Love waves and maxima along the sliding axis for Rayleigh waves. This pattern is well captured by the CSF model. Examples of typical waveforms and the modeled fits are shown in Figure 2. In all cases, the filtered seismograms have a harmonic character (see Figure 2) and have signals not far above the noise. This makes it difficult to distinguish between two sources that are offset in time by half the dominant period and reversed in polarity with respect to each other. As the dominant period is typically around 50 s, the best fit solution usually only has a small improvement in misfit over a solution with around 25 s delay or 25 s advance. These delayed or advanced solutions then have nearly opposite polarity. As an example of such ambiguity, the 15 September 2000 event has a best fit residual variance of r = 0.364, a delay of 25.3 s gives r = 0.439, and an advance of 25.2 s gives r = 0.550. The sliding directions in all three cases are nearly horizontal and the delayed and advanced solutions point 173° and 176° (respectively) from that of the best fit solution. Except for this possible 180° ambiguity, the direction of sliding is well constrained by the characteristic two-lobed radiation pattern. Similarly, except for the possible delay or advance by half the dominant period (20–30 s), the centroid time of the event is well constrained (to within 2–3 s) by the phase of the seismic signals.

[11] Because of the many sources of noise and our lack of a priori knowledge of these sources of uncertainty, it is difficult to assess quantitatively the uncertainty in retrieved parameters resulting from our analysis. However, *Smith and Ekström* [1997] show that CMT inversions have a one sigma absolute uncertainty in horizontal location of approximately 25 km. Our CSF inversions rely on the same algorithm with slight modification to the source model so we expect our uncertainties to be roughly the same. The excitation of seismic waves is modeled within PREM [*Dziewonski and Anderson*, 1981], a 1D seismic velocity model with a water layer at 0–3 km depth and an upper crust at 3–15 km depth. Since excitation functions do not change substantially in the PREM upper crust, we choose to model all events at 12 km depth, following the practice in standard CMT analysis of very shallow earthquakes [*Dziewonski et al.*, 1981; *Ekström et al.*, 2005]. All events are well fit with model depths anywhere between 3 and 15 km, and retrieved source parameters are identical to within uncertainties. This is not meant to imply source depths are greater than 3 km (we interpret all glacial earthquakes to be shallower than 3 km), but is a limitation of the sensitivity of long-period seismic waves to source depth. All modeled vertical forces are small, with dip angles mostly shallower than 10° and all shallower than 20°. We

Table 1. Glacial Earthquake Parameters[a]

Latitude, °N	Longitude, °E	Amplitude, $\times 10^{14}$ kg m	Direction, °E of N	Time Lag From Detection Time, s	Detection Parameters									Region Number
					Year	Month	Day	Hour	Minute	Second	Latitude	Longitude	Surface Wave Magnitude	
68.63	−32.94	1.97	−23.9	3.95	1993	1	24	10	21	4.00	68.50	−33.50	5.1	1
65.23	−40.87	0.63	−38.5	−10.52	1993	7	26	12	26	40.00	65.75	−41.25	4.9	3
68.58	−32.90	0.75	−48.8	9.84	1993	8	5	2	0	40.00	68.75	−32.75	4.9	1
68.66	−33.12	0.60	−49.6	−10.65	1993	8	24	2	56	0.00	67.00	−35.00	4.8	1
66.38	−37.72	0.35	100.0	14.83	1993	10	19	21	10	0.00	66.50	−37.50	4.8	2
68.66	−32.93	1.03	147.8	2.60	1993	11	30	7	33	52.00	67.50	−33.50	5.0	1
68.68	−32.93	1.18	−22.6	21.40	1993	12	10	15	24	56.00	67.25	−34.25	5.0	1
68.62	−32.96	0.60	−52.2	13.09	1994	3	31	0	7	4.00	68.50	−33.50	4.8	1
65.35	−41.03	0.58	131.2	13.07	1994	4	6	18	1	28.00	65.75	−41.25	4.8	3
65.23	−41.12	0.15	−59.9	−3.96	1994	8	16	8	58	48.00	65.25	−40.75	4.7	3
68.63	−32.88	1.09	104.6	−9.15	1994	8	21	8	36	48.00	68.50	−33.50	5.0	1
71.92	−28.45	0.39	81.0	4.25	1994	8	21	9	46	56.00	72.50	−28.50	4.8	0
71.77	−51.90	0.30	−121.6	17.71	1994	8	26	6	11	28.00	72.25	−51.25	4.9	6
68.65	−32.99	0.77	150.7	−12.19	1994	11	26	4	11	4.00	69.25	−31.25	4.9	1
68.59	−32.78	0.17	123.2	−0.40	1995	7	18	5	30	56.00	69.00	−31.00	4.9	1
68.62	−32.78	0.48	−33.2	10.72	1995	7	24	23	3	52.00	67.25	−33.25	4.8	1
71.92	−29.58	0.65	−72.3	5.45	1995	8	3	4	21	52.00	72.75	−28.75	4.9	0
68.63	−33.22	0.83	105.1	−3.64	1995	9	4	0	25	12.00	69.00	−33.00	5.0	1
68.56	−32.90	0.71	149.0	−4.71	1995	10	6	3	7	36.00	68.00	−38.00	4.9	1
68.64	−32.92	1.70	145.6	0.70	1995	11	8	22	20	32.00	70.50	−27.50	5.0	1
73.53	−54.76	0.40	60.7	−17.12	1995	11	12	2	27	20.00	73.75	−56.25	4.7	5
68.54	−32.97	1.34	144.6	0.01	1995	12	11	9	35	44.00	68.50	−31.50	5.0	1
68.55	−33.06	0.68	133.8	−6.15	1996	1	28	16	14	8.00	68.25	−32.75	4.9	1
66.53	−38.44	0.40	74.8	−17.24	1996	5	14	13	50	16.00	66.25	−38.25	4.8	2
68.76	−33.69	0.60	129.2	−1.34	1996	6	26	18	29	28.00	68.25	−33.25	4.9	1
68.67	−33.05	1.02	−27.1	22.97	1996	7	19	18	37	28.00	67.50	−33.50	4.9	1
66.25	−38.18	0.31	102.9	−8.62	1996	7	25	23	26	8.00	66.25	−37.75	4.8	2
66.47	−38.10	0.28	−73.5	3.51	1996	8	8	2	47	4.00	68.00	−38.00	4.7	2
68.60	−33.22	1.52	−41.0	13.70	1996	10	4	22	4	48.00	69.25	−32.25	4.9	1
66.43	−38.18	0.52	−90.0	10.24	1996	11	6	3	46	0.00	67.50	−38.50	4.8	2
66.47	−38.08	0.58	−94.3	16.47	1996	11	30	13	35	44.00	65.75	−38.25	4.9	2
68.74	−32.93	1.09	−79.1	−18.16	1996	12	7	1	42	32.00	66.75	−34.25	5.1	1[b]
68.63	−32.87	0.46	149.5	−0.77	1997	3	16	14	52	40.00	68.25	−33.25	4.9	1
71.77	−51.60	0.47	−104.4	15.25	1997	3	28	2	28	16.00	71.75	−51.25	4.9	6
68.72	−32.94	0.33	−39.9	9.84	1997	4	7	7	0	32.00	68.25	−33.25	4.8	1
65.31	−41.16	0.32	−51.2	5.89	1997	5	4	16	28	48.00	65.75	−40.25	4.8	3
68.56	−32.67	0.32	146.3	−10.21	1997	7	15	6	54	48.00	69.00	−33.00	4.8	1
71.81	−29.17	0.45	−109.4	12.09	1997	8	15	12	1	28.00	72.25	−30.25	4.9	0
68.65	−32.91	0.68	−27.6	7.15	1997	8	20	13	28	40.00	68.75	−32.75	4.9	1
71.78	−51.63	0.63	−113.9	1.85	1997	9	6	3	45	52.00	71.75	−52.25	5.0	6
68.64	−33.10	0.94	129.4	−0.68	1997	9	12	3	59	20.00	69.25	−32.75	5.0	1[b]
68.74	−33.36	0.73	128.0	0.21	1997	9	24	22	9	12.00	68.25	−33.25	4.9	1[b]
66.37	−38.30	0.38	115.3	−10.36	1997	10	1	17	41	28.00	67.00	−39.00	4.7	2
65.36	−41.20	0.21	−51.9	9.81	1998	5	1	22	19	36.00	65.75	−40.75	4.7	3
66.40	−38.02	0.22	92.3	2.85	1998	6	3	15	9	28.00	66.50	−38.50	4.8	2
69.32	−50.08	0.46	−105.4	19.51	1998	6	6	16	39	44.00	69.75	−49.75	4.9	7
69.34	−50.27	0.46	−113.5	9.72	1998	6	11	0	18	56.00	69.75	−50.75	4.9	7
66.43	−38.08	0.34	86.1	−11.56	1998	6	13	18	11	52.00	66.25	−38.25	4.8	2
69.14	−49.30	0.40	−90.1	11.88	1998	6	29	15	16	56.00	69.50	−49.50	4.7	7
66.37	−38.02	0.31	77.8	−7.03	1998	7	8	9	31	12.00	66.75	−38.25	4.8	2
69.32	−50.05	0.29	−100.5	21.05	1998	7	21	6	30	16.00	69.00	−49.00	4.8	7
69.28	−49.30	0.27	75.9	31.80	1998	7	25	0	49	4.00	69.00	−49.00	4.7	7
69.29	−49.77	0.30	94.4	−10.61	1998	7	28	0	37	28.00	69.50	−49.50	4.8	7
68.63	−32.75	0.24	−76.1	9.72	1998	9	20	3	36	0.00	68.25	−33.75	4.7	1
68.92	−32.98	0.97	−21.2	15.93	1998	10	13	22	12	48.00	68.75	−32.25	5.0	1
68.80	−33.06	0.72	154.1	−15.16	1998	10	27	3	30	24.00	68.75	−32.75	5.0	1
68.74	−32.95	0.52	−32.0	12.18	1999	1	22	14	0	48.00	68.25	−34.25	4.8	1
71.83	−51.54	0.64	−112.6	0.49	1999	4	19	23	0	24.00	71.75	−51.25	4.9	6
71.81	−51.73	0.57	57.3	21.74	1999	4	21	3	49	36.00	69.25	−51.75	4.8	6
69.30	−49.63	0.59	−64.7	2.73	1999	4	24	12	17	28.00	69.50	−50.50	4.9	7[b]
69.20	−49.88	0.26	31.3	8.59	1999	5	2	23	16	24.00	69.75	−49.75	4.7	7
69.27	−49.63	0.28	−110.3	13.06	1999	5	20	11	34	56.00	68.75	−49.75	4.8	7
69.32	−50.06	0.45	−144.1	−13.94	1999	6	9	14	49	4.00	70.50	−49.50	4.8	7
66.58	−38.23	0.34	86.6	−4.74	1999	7	18	6	30	32.00	66.50	−38.50	4.8	2
69.28	−49.84	0.34	−54.1	11.68	1999	8	14	14	4	56.00	68.75	−50.25	4.9	7
66.44	−38.03	0.39	83.9	−5.69	1999	9	2	9	16	56.00	66.75	−38.25	4.8	2
68.66	−32.83	0.82	−24.9	21.32	1999	10	8	9	34	56.00	68.25	−32.75	4.9	1
68.78	−33.70	0.45	−46.3	17.42	1999	11	15	22	56	8.00	68.25	−32.75	4.8	1
68.61	−32.67	0.61	150.1	−5.70	1999	11	15	23	6	16.00	68.25	−32.75	4.9	1
66.29	−38.80	0.34	−104.2	10.27	1999	12	21	4	40	16.00	65.50	−37.50	4.7	2
68.62	−32.90	0.68	−30.9	−7.54	2000	3	3	14	41	12.00	69.25	−30.75	4.8	1

Table 1. (continued)

Latitude, °N	Longitude, °E	Amplitude, $\times 10^{14}$ kg m	Direction, °E of N	Time Lag From Detection Time, s	Detection Parameters									
					Year	Month	Day	Hour	Minute	Second	Latitude	Longitude	Surface Wave Magnitude	Region Number
68.75	−33.49	0.60	−40.3	−4.68	2000	3	3	14	57	12.00	68.50	−35.50	4.9	1
68.70	−32.78	0.62	−42.6	0.98	2000	6	12	9	37	4.00	69.50	−31.50	4.8	1
71.98	−28.32	0.45	73.5	6.20	2000	7	2	10	36	48.00	71.75	−28.75	4.8	0
68.61	−32.81	1.22	−34.8	−5.08	2000	7	21	19	2	40.00	67.75	−34.25	5.0	1[b]
75.40	−58.14	0.45	−145.8	0.04	2000	8	16	21	24	48.00	75.50	−59.50	4.9	4
65.30	−41.32	0.41	−41.5	−5.50	2000	9	4	11	57	28.00	66.50	−41.50	4.8	3
66.28	−38.05	0.32	93.0	−4.43	2000	9	15	7	4	32.00	66.25	−37.75	4.8	2
73.53	−55.33	0.56	82.6	3.29	2000	9	17	2	18	8.00	73.50	−56.50	4.8	5
68.69	−32.94	0.63	−32.9	0.52	2000	10	20	2	1	4.00	69.00	−33.00	4.9	1
66.42	−37.95	0.33	−107.1	16.44	2001	2	7	5	36	8.00	65.75	−37.75	4.8	2
73.07	−54.65	0.33	−121.3	15.45	2001	7	2	1	14	24.00	72.75	−54.25	4.7	5
66.48	−37.96	0.35	−106.1	8.19	2001	7	6	3	25	44.00	66.50	−38.50	4.8	2
75.84	−58.22	0.32	−10.9	10.96	2001	8	11	6	27	28.00	75.75	−59.25	4.8	4
68.67	−32.93	0.78	148.5	9.26	2001	9	3	13	1	12.00	68.50	−34.50	4.9	1
68.67	−33.05	0.55	131.0	−5.05	2001	10	1	16	37	36.00	68.75	−33.75	4.9	1
73.15	−54.21	0.21	−115.6	0.63	2001	10	24	17	24	56.00	72.50	−54.50	4.6	5
68.59	−33.03	1.15	−20.5	2.55	2001	11	29	2	46	40.00	67.75	−32.25	5.0	1[b]
68.69	−32.98	0.48	−35.1	−43.96	2001	12	20	7	27	4.00	69.00	−27.00	4.8	1
71.81	−51.77	0.32	−93.7	47.89	2001	12	21	3	13	36.00	72.75	−53.75	4.8	6[b]
66.45	−38.36	0.27	108.0	4.13	2001	12	26	19	39	52.00	66.25	−38.75	4.7	2
68.61	−32.78	0.87	−18.1	9.79	2001	12	28	17	19	36.00	68.75	−33.25	5.0	1
68.62	−33.04	0.78	−46.5	−2.41	2002	2	27	15	43	4.00	69.50	−30.50	4.9	1
68.65	−33.00	0.76	−37.8	1.97	2002	4	4	22	49	4.00	68.75	−33.25	4.9	1
66.44	−38.22	0.29	−92.6	−11.36	2002	4	19	21	50	8.00	67.25	−38.25	4.7	2
66.44	−38.30	0.35	89.2	−7.92	2002	5	1	10	13	44.00	66.25	−38.25	4.8	2
66.40	−38.20	0.25	−72.2	3.51	2002	5	12	18	6	24.00	66.75	−38.75	4.7	2
66.44	−38.21	0.27	110.6	2.12	2002	6	8	4	31	44.00	66.25	−38.25	4.7	2
66.50	−38.05	0.22	76.3	5.75	2002	6	8	18	2	16.00	66.25	−38.25	4.7	2
73.13	−54.25	0.47	−103.8	−8.62	2002	6	18	22	2	8.00	73.25	−57.25	4.8	5
73.12	−54.52	0.45	−120.4	−1.60	2002	7	14	5	18	32.00	73.00	−55.00	4.8	5
75.54	−58.26	0.29	−149.9	1.02	2002	7	19	0	42	16.00	75.00	−57.00	4.7	4
66.38	−38.34	0.30	99.8	−2.93	2002	8	3	10	13	4.00	66.75	−38.25	4.8	2
68.80	−33.53	0.36	101.8	−6.84	2002	9	20	2	0	16.00	68.50	−33.50	4.9	1
68.68	−33.15	0.38	−81.1	11.56	2002	9	26	3	46	16.00	69.00	−33.00	4.8	1
76.03	−59.44	0.29	45.0	−1.86	2002	10	2	22	25	44.00	76.50	−63.50	4.8	4
75.53	−57.83	0.35	−140.1	6.99	2002	11	14	12	50	56.00	75.75	−59.25	4.8	4
68.68	−33.32	0.69	132.8	1.65	2003	2	3	21	44	0.00	68.50	−32.50	5.0	1
71.89	−51.21	0.39	−116.2	12.27	2003	2	17	19	30	40.00	71.50	−52.50	4.8	6
75.92	−59.71	0.42	47.6	−13.44	2003	3	10	21	17	36.00	75.50	−57.50	4.9	4
75.64	−58.08	0.31	−141.5	7.07	2003	3	26	9	21	4.00	75.75	−57.75	4.7	4
71.81	−51.92	0.41	63.6	9.41	2003	4	1	8	29	44.00	71.00	−53.00	4.8	6
72.16	−28.65	0.55	53.4	−0.07	2003	7	26	4	41	44.00	72.25	−28.75	4.8	0
66.30	−38.43	0.46	85.9	−1.63	2003	8	3	23	40	40.00	66.25	−37.75	4.9	2
68.68	−33.00	0.41	−31.7	8.93	2003	8	5	14	0	24.00	68.50	−33.50	4.8	1
68.47	−32.88	0.64	−44.0	3.65	2003	8	13	8	51	12.00	68.25	−34.75	5.0	1
74.90	−56.18	0.28	−123.1	−0.20	2003	8	14	23	30	24.00	75.00	−57.00	4.7	4
75.45	−58.10	0.32	−152.2	−4.63	2003	8	30	5	49	28.00	75.75	−58.75	4.7	4
76.04	−59.81	0.43	63.2	15.78	2003	9	20	20	31	20.00	75.75	−60.25	4.8	4
68.60	−32.97	0.36	159.5	8.08	2003	9	24	1	1	12.00	69.25	−32.25	4.8	1
68.69	−33.09	0.81	−32.6	16.45	2003	9	24	1	32	0.00	69.25	−32.75	5.0	1
66.49	−38.52	0.42	95.4	12.36	2003	10	2	9	7	4.00	67.25	−37.25	4.8	2
68.56	−32.85	1.11	−40.1	23.86	2003	10	5	3	7	52.00	68.50	−33.50	5.0	1
66.37	−38.38	0.56	101.6	3.07	2003	10	12	21	12	40.00	66.50	−38.50	4.9	2
68.75	−32.87	0.52	148.2	−1.78	2003	10	18	16	10	56.00	68.50	−33.50	5.0	1
75.99	−59.24	0.35	−136.6	−3.17	2003	10	19	9	23	44.00	76.25	−60.75	4.8	4
66.40	−38.24	0.43	108.1	−8.15	2003	11	9	4	17	52.00	66.25	−38.25	4.8	2
75.87	−60.00	0.23	27.8	11.24	2004	1	7	14	37	4.00	75.75	−58.75	4.7	4
67.87	−33.51	0.20	−82.9	18.32	2004	1	27	6	15	52.00	68.25	−33.75	4.7	1
66.37	−38.54	0.21	91.7	10.73	2004	3	16	14	1	36.00	66.50	−38.50	4.6	2
73.56	−54.35	0.12	−175.6	−16.30	2004	4	11	4	7	36.00	73.00	−55.00	4.6	5
66.43	−38.06	0.50	−93.6	20.56	2004	5	26	12	0	16.00	66.25	−38.75	4.8	2
75.55	−58.34	0.32	−146.6	−15.72	2004	6	3	4	38	48.00	75.75	−59.25	4.8	4
66.44	−38.42	0.70	96.5	−2.72	2004	6	25	5	58	56.00	66.50	−38.50	4.9	2
66.51	−38.84	0.32	84.2	−7.79	2004	6	25	6	5	28.00	66.25	−38.75	4.9	2
71.83	−51.58	0.33	40.7	−2.78	2004	7	2	6	15	20.00	71.25	−51.75	4.8	6
66.38	−38.18	0.28	82.4	1.89	2004	7	6	10	15	12.00	66.25	−38.25	4.8	2
66.31	−38.30	0.27	97.3	3.14	2004	7	6	10	22	48.00	65.75	−37.75	4.7	2
66.45	−38.98	0.44	−88.4	19.21	2004	7	21	12	33	36.00	66.75	−38.25	4.8	2
68.61	−32.84	0.29	−42.7	−1.11	2004	8	1	9	27	4.00	69.00	−33.00	4.8	1
66.41	−38.26	0.36	112.3	3.81	2004	8	11	7	22	40.00	66.75	−39.25	4.8	2

Table 1. (continued)

Latitude, °N	Longitude, °E	Amplitude, $\times 10^{14}$ kg m	Direction, °E of N	Time Lag From Detection Time, s	Detection Parameters								Surface Wave Magnitude	Region Number
					Year	Month	Day	Hour	Minute	Second	Latitude	Longitude		
72.01	−28.60	0.60	−116.9	3.67	2004	8	12	13	8	8.00	72.75	−29.75	4.9	0
66.40	−38.15	0.37	101.0	2.96	2004	8	13	19	34	0.00	66.25	−38.25	4.9	2
75.71	−58.16	0.39	45.8	12.12	2004	8	22	14	9	44.00	75.75	−57.25	4.7	4
76.07	−59.39	0.33	−113.3	1.63	2004	8	26	17	0	8.00	75.75	−58.25	4.8	4
68.67	−33.20	0.33	−48.9	−18.84	2004	9	20	5	11	4.00	68.50	−33.50	4.8	1
73.06	−54.46	0.35	−142.2	−3.93	2004	9	26	7	46	16.00	72.75	−54.25	4.8	5
68.67	−33.27	0.74	−96.7	6.10	2004	11	1	16	39	12.00	69.25	−32.25	5.0	1
66.45	−38.16	0.29	112.9	−3.35	2004	11	2	22	6	40.00	67.00	−37.00	4.8	2
75.92	−59.74	0.43	38.6	22.69	2004	11	20	7	29	28.00	75.75	−60.75	4.9	4
75.98	−59.84	0.37	44.8	7.69	2004	11	24	3	44	24.00	76.25	−60.75	4.8	4
68.74	−33.53	0.30	92.3	−9.62	2004	11	24	20	55	12.00	69.50	−33.50	4.7	1
76.09	−59.51	0.43	164.2	6.13	2004	12	16	14	53	12.00	76.25	−61.75	4.8	4
75.99	−59.60	0.37	−130.1	3.91	2004	12	30	17	6	0.00	76.25	−60.75	4.8	4
75.63	−57.88	0.49	−50.9	−5.70	2005	1	2	7	26	8.00	75.50	−59.50	4.8	4
68.69	−33.22	1.00	−81.9	8.74	2005	1	12	20	39	12.00	68.75	−33.25	5.1	1
66.53	−38.49	0.84	124.0	−0.16	2005	2	11	6	55	20.00	66.75	−38.75	5.0	2
66.50	−38.42	0.59	116.6	−1.41	2005	2	19	13	29	28.00	66.50	−38.50	4.8	2
68.65	−32.60	0.35	146.9	−5.57	2005	3	20	8	5	4.00	68.50	−32.50	4.8	1
66.42	−38.01	0.39	99.8	−7.86	2005	4	5	13	3	28.00	66.50	−38.50	4.9	2
68.81	−32.92	0.45	164.5	2.67	2005	4	6	16	41	20.00	68.75	−32.75	4.9	1
66.48	−38.72	0.51	−63.3	26.92	2005	4	23	2	10	8.00	66.75	−37.75	5.0	2[b]
68.68	−33.07	0.49	−12.7	−9.87	2005	4	26	6	13	28.00	68.25	−33.75	4.8	1
66.44	−38.04	0.52	120.7	−1.63	2005	5	12	17	23	20.00	67.25	−37.25	5.0	2
66.47	−38.22	0.68	−66.7	12.01	2005	5	12	19	16	56.00	66.25	−38.25	4.9	2
75.91	−59.95	0.40	−131.3	1.13	2005	6	11	16	10	48.00	76.25	−61.75	4.8	4
66.52	−38.54	0.43	110.0	−8.14	2005	6	16	13	57	44.00	66.50	−39.50	4.9	2
66.39	−38.30	0.51	140.9	11.22	2005	7	11	21	53	12.00	65.50	−38.50	4.8	2
71.81	−51.77	0.50	67.8	−15.98	2005	7	17	2	30	56.00	71.50	−51.50	4.8	6
65.24	−41.48	0.37	−65.6	16.83	2005	7	28	0	45	4.00	65.25	−41.25	4.8	3
72.01	−28.45	0.43	−121.0	12.81	2005	7	28	12	22	40.00	72.25	−27.75	4.8	0
69.32	−49.59	0.41	−99.6	−2.59	2005	7	30	20	28	56.00	69.25	−49.25	4.8	7
71.90	−28.38	0.37	−146.7	16.51	2005	8	2	13	28	40.00	72.25	−29.75	4.8	0
72.89	−54.23	0.26	52.5	−1.71	2005	8	3	0	58	0.00	73.50	−53.50	4.7	5
66.42	−38.29	0.50	92.3	−6.27	2005	8	11	6	1	36.00	66.75	−38.75	4.9	2
66.42	−38.21	0.23	69.5	−3.34	2005	8	11	6	40	0.00	65.25	−38.25	4.7	2
77.62	−66.78	0.39	82.7	−5.98	2005	8	12	19	30	56.00	77.50	−66.50	4.8	4
66.46	−38.27	0.48	−60.2	17.74	2005	8	14	3	33	12.00	65.75	−38.25	4.9	2
69.22	−49.68	0.39	−108.7	−5.74	2005	8	16	0	56	40.00	69.75	−49.75	4.8	7[b]
76.03	−59.46	0.46	53.3	−21.81	2005	8	18	1	39	4.00	76.25	−60.75	4.8	4
66.39	−38.27	0.25	54.3	8.80	2005	8	20	7	54	40.00	67.50	−38.50	4.7	2
67.74	−33.14	0.16	−113.1	7.64	2005	9	18	15	1	52.00	69.50	−34.50	4.7	1
68.61	−33.16	0.80	−62.6	−0.68	2005	9	20	10	7	44.00	69.50	−32.50	5.0	1
74.64	−56.46	0.35	−124.8	−10.69	2005	10	10	20	15	12.00	75.25	−56.75	4.8	4

[a]The first five columns result from CSF waveform inversion. Regions: 0, DJ; 1, K; 2, H; 3, SEG; 4, northern NWG; 5, southern NWG; 6, RI; 7, JI. The dip angles for all events are less than 20°. The depths of all events are constrained at 12 km as discussed in the text.
[b]Complex events that are not well fit with the simple model.

do not trust the precise values of these shallow dips so we shall not discuss them further. Since uncertainties due to imperfect knowledge of 3D Earth structure are similar for events in the same locality, we expect our relative location uncertainties to be smaller than the absolute uncertainty. On the basis of numerical experiments done to test the sensitivity of including different data and using different model parameters, we estimate our relative location uncertainty to be 4–15 km, relative sliding direction uncertainty to be 5°–20°, and relative amplitude uncertainty to be 10–80%. For comparison, *Ekström et al.* [2003, 2006] report relative location uncertainties of approximately 100 km and 20 km, respectively. Lower signal-to-noise results in fewer data used and substantial noise contributing to inversions so that small events have uncertainties on the high end of all estimated uncertainties except for amplitude uncertainties. As discussed earlier, the amplitude uncertainties may be systematic, with small events being smaller than estimated and large events being larger than estimated.

[12] Finally, a few events are not well modeled with the symmetric boxcar CSF. Many of these complex events are much better modeled as two CSFs. The need for two CSFs may imply a large delay between the acceleration and deceleration phase of the events. Since we filter our data at 35–75 s, 40–100 s, or 50–150 s period, accelerations lasting longer than 75, 100, or 150 s (respectively) will not be observed well. Therefore we may be observing two shorter-period phases within a longer event. These shorter phases may not be equal in magnitude or opposite in direction since only the sum of all accelerations is constrained to be zero. Alternatively, it may imply two separate events, the second of which was likely triggered by the first. A final alternative is that the landslide source model simply is not a good description of these events. Although we list

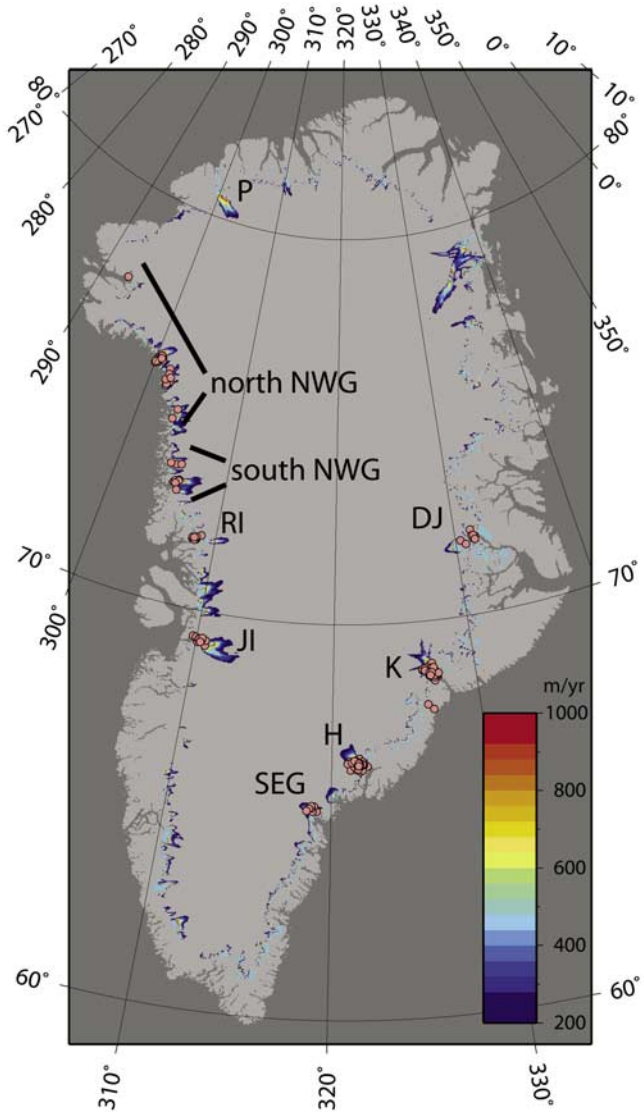

Figure 3. Locations of the 184 glacial earthquakes resulting from source analysis, plotted as pink circles. The background colors represent Greenland ice sheet balance velocities from *Bamber et al.* [2001] in units of m/yr. To emphasize regions of high ice flow velocity, velocities less than 200 m/yr are not plotted. Region names are Daugaard Jensen (DJ), Kangerdlugssuaq (K), Helheim (H), southeast Greenland (SEG), Jakobshavn Isbrae (JI), Rinks Isbrae (RI), and northwest Greenland (NWG).

CSF model parameters for these complex events, given the above discussion, these parameters may not be particularly meaningful. Further study is needed to fully understand these complex events. They are identified by footnote b in Table 1.

3. Source Analysis Results

[13] Our source analysis results in CSF amplitudes, force directions, and a more precise determination of centroid times and locations. A summary of these parameters for all 184 Greenland glacial earthquakes are listed in Table 1. Figure 3 displays the locations of all Greenland earthquakes superimposed on a map of Greenland ice sheet balance velocities [*Bamber et al.*, 2001]. In comparison to the original location estimates from the earthquake detection algorithm (see Table 1), we observe strong clustering of events (see Figure 4). Comparison with Greenland ice sheet balance velocities (see Figure 3) shows that we observe glacial earthquakes only in regions where the ice flow speeds are above 800 m/yr. The converse is not true since there are regions of high ice flow, such as Petermann Glacier (denoted P in Figure 3), where no glacial earthquakes have been detected yet.

[14] The locations in which we observe glacial earthquakes can be grouped into roughly seven distinct regions, all of which are coincident with ice streams or outlet glaciers. In this paper, we denote these seven regions as Daugaard Jensen (DJ), Kangerdlugssuaq (K), Helheim (H), southeast Greenland (SEG), Jakobshavn Isbrae (JI), Rinks Isbrae (RI), and northwest Greenland (NWG) (see Figure 3). The NWG region includes the Steenstrup Glacier, Dietrichson Glacier, Sverdrup Glacier, Kong Oscar Glacier, and a number of other smaller outlet glaciers. Of the 184 events, 8 occur in DJ, 64 in K, 49 in H, 7 in SEG, 24 in northern NWG, 9 in southern NWG, 10 in RI, and 13 in JI. Of the 64 events that occur in the K region, all but two occur in the K Glacier with the two outliers occurring in a nearby outlet glacier (these two events are not used in the statistical descriptions of the K region). All of the events in the DJ, H, JI and RI regions occur within the glacier with the same name (to within location errors). All of the events in region H and all 62 events in the K Glacier occur within a 60 by 40 km area.

[15] Figures 5 and 6 show detailed views of the regions, with force amplitudes and directions denoted. In all cases, the directions of the modeled sliding axes are consistent with the direction of glacial ice flow (see Figure 7). This is the sliding direction expected, thus validating the use of the landslide model. Many of the arrowheads point in the direction opposite the expected one. As discussed in section 2, this is possibly an artifact of the simple symmetric boxcar model used, and not reflective of "upslope" sliding events. This is our preferred interpretation. The rest of the scatter in the direction of the modeled forces we attribute either to real variations in average force directions or to errors resulting from the modeling. As discussed earlier, the errors for many of the smaller events are substantial (estimated to be up to 20°) so it is difficult to distinguish between the two contributions to the scatter in direction.

4. Analysis and Interpretation

[16] The data set resulting from our source analysis contains a wealth of information that can be used to further characterize glacial earthquakes. Here, we analyze the temporal, spatial, and size distribution of the events.

[17] As discussed in *Ekström et al.* [2006], there is a seasonal variation in when glacial earthquakes occur, with a peak of activity in northern summer (July, August and September) and a dearth of events in northern winter (January and February having a factor of six fewer events than August). This seasonality suggests that temperature is (indirectly) a factor in determining when glacial earthquakes occur. Examining each region separately, we find distinct differences between them (see Figure 8). Region DJ has a

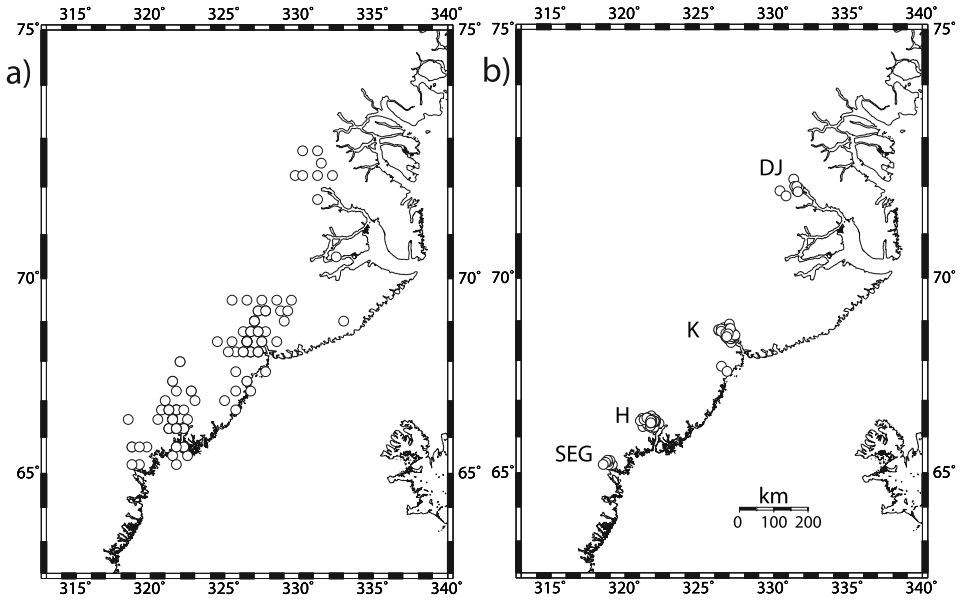

Figure 4. (a) Original locations of all of the east Greenland events based on the surface wave detection algorithm. (b) Revised locations of the same events from the surface wave waveform analysis. Region names are as in Figure 3.

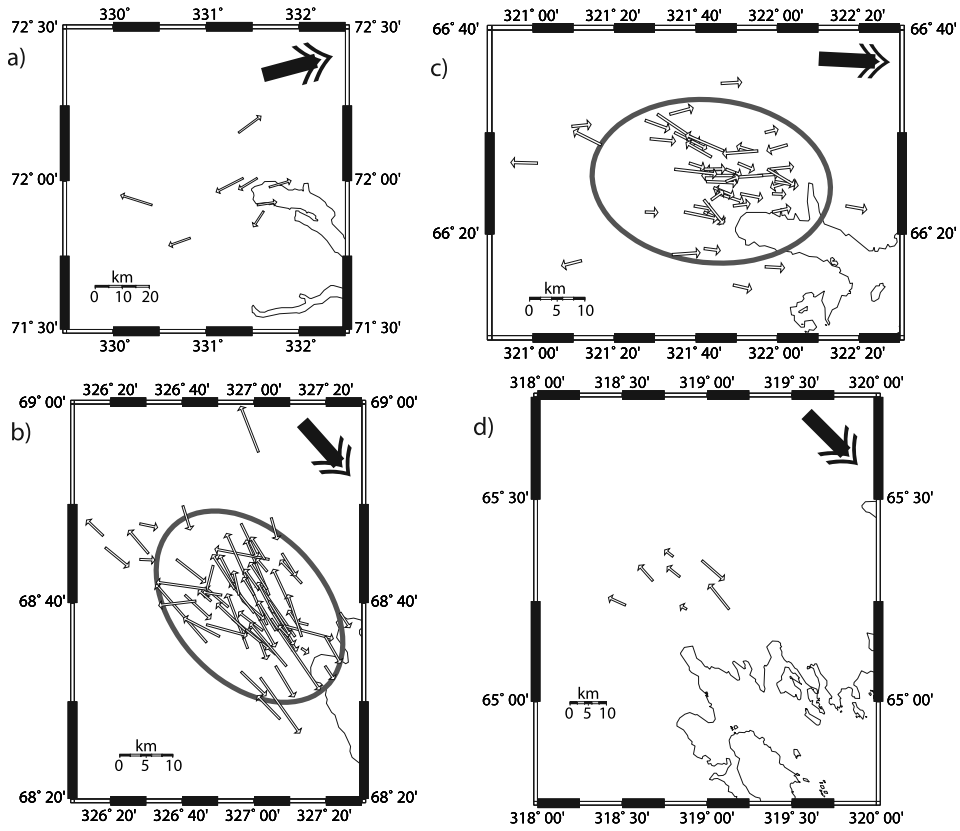

Figure 5. Modeled force directions for the (a) Daugaard Jensen (DJ) region, (b) Kangerdlugssuaq (K) region, (c) Helheim (H) region, and (d) southeast Greenland (SEG) region. Arrows point in the direction of initial ground acceleration, centroid locations are defined by the location of the arrow tails, and arrow length is proportional to the amplitude of the event. The wide double-headed arrows represent the approximate direction of local glacial flow. The ellipses denote a 2 sigma location ellipse, as discussed in section 4.

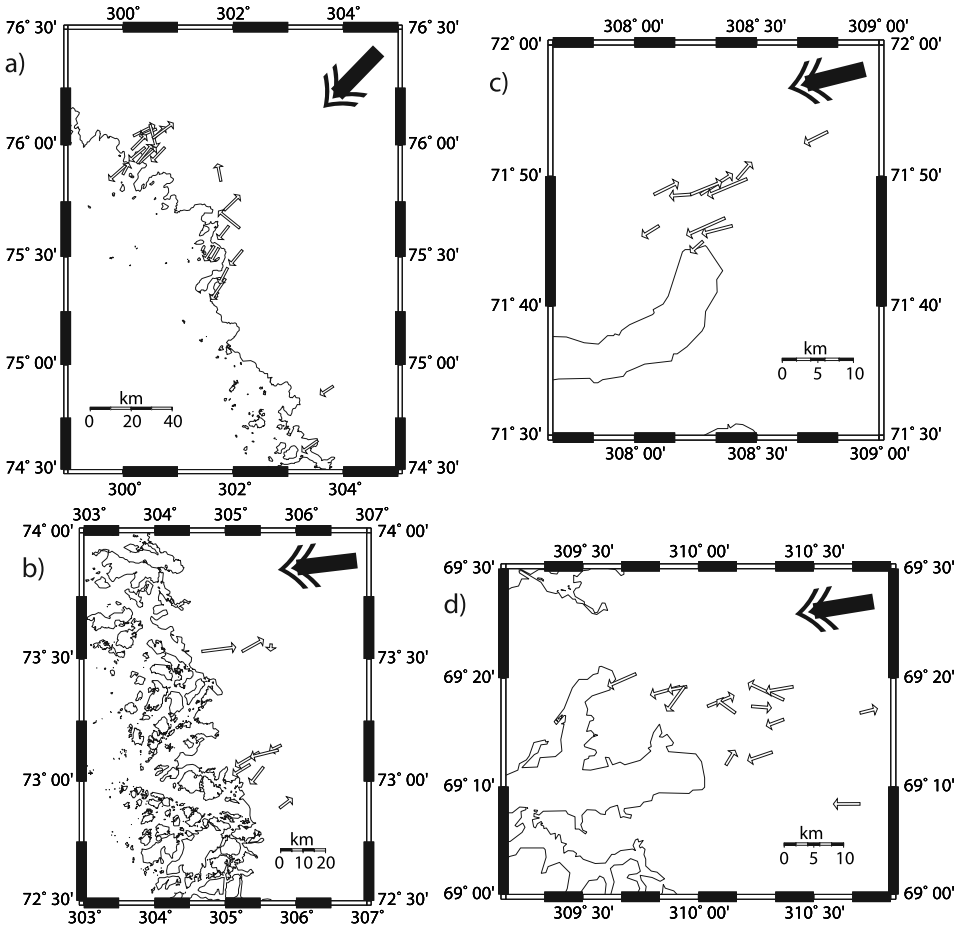

Figure 6. Modeled force directions for the (a) northern northwest Greenland (NWG) region, (b) southern NWG region, (c) Rinks (RI) region, and (d) Jakobshavn (JI) region. Figure 6a does not include the one event occurring north of 77°N. Symbols are as in Figure 5.

single (sharp) peak in activity in August; K has a peak in September, may have a second peak (March–April), but has activity year-round that decreases to zero in May and increases afterward; H has a broad peak in June–August, may have a second peak (October–November), but also has activity year-round that deceases to zero in January; RI has two peaks of activity, with activity February–April and July–September; SEG also seems to have two peaks in activity; JI has a single peak in June–July; NWG has a sharp peak in August although other features may be obscured due to averaging over multiple outlet glaciers. Some of this variability may be due to statistics of small numbers, but some features are statistically significant. For example, using a two-sample t test, we reject at the 95% confidence level the hypothesis that the peak in activity in region K and region H occur at the same time. In contrast to the clear progression to warmer temperatures with decreasing latitude observed in regional weather data [*Cappelen et al.*, 2001], seasonal glacial earthquake activity does not show a clear latitudinal dependence.

[18] All of the events in the JI region prior to 2005 occurred in the summer months of 1998 and 1999, temporally coincident with very large accelerations in the average JI velocity [*Luckman and Murray*, 2005; *Joughin et al.*, 2004]. The correspondence is even more striking when compared with GPS motion upstream of JI from *Zwally et al.* [2002], as the JI glacial earthquakes precede the observed episodes of accelerated motion by one or two months. The coincidence of surface melting with the spikes in velocity [*Zwally et al.*, 2002] gives a natural interpretation of glacial earthquakes as being influenced by meltwater reaching the glacier bed; the fact that the glacial earthquakes occur earlier could be interpreted as a consequence of melting occurring earlier downstream. However, observations of increased calving and retreat of JI during the same years [*Luckman and Murray*, 2005; *Joughin et al.*, 2004] complicate this interpretation.

[19] A second temporal trend in the data is the dramatic increase in the total number of events since 2002, with more events detected in each successive year since 2002 and resulting in more than twice as many events in 2005 as compared with any year prior to 2003 [*Ekström et al.*, 2006]. This dramatic increase, however, has not occurred in all regions (see Figure 9). The K region has no distinguishable increase in events over time and is consistent with 4.8 ± 1.2 events per year for the entire detection period. Most of the dramatic increase is due to changes in region H and NWG. In region H, there was a small peak in activity from 1996 to 1999, and from 2000 to the present there has been substantial increase to 10 or more events per year.

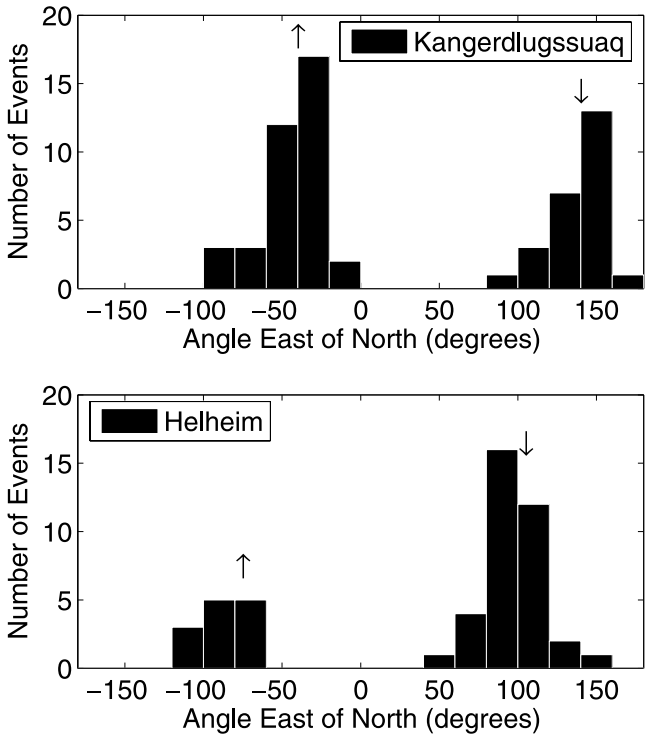

Figure 7. Force directions for regions K and H, compared to glacier orientation. Up arrows correspond to the upstream direction, and down arrows correspond to the downstream direction of glacial flow, estimated from *Rignot et al.* [2004].

Region NWG has a more striking change in that the northern part of region NWG did not have a single event before 2000 but has had a steadily increasing number of events until 2005. 2005 had fewer events than 2004, suggesting that the peak in activity may have passed. The southern part of region NWG displays similar behavior to the northern part but without as large of a contrast between the pre-2000 and post-2000 years.

[20] Other temporal trends exist but are not as compelling due to the small number of events. One such trend is the decrease in size of events in region K, especially of the largest events, with the four largest events occurring in the first four years of the study period (1993–1996). Another such trend is the increase in latitude of the highest-latitude event through the study period, going from 68.7°N in 1993 to 73.5°N in 1995 to 75.4°N in 2000 to 77.6°N in 2005. This increase in northerly extent correlates well with the decrease in southerly extent of arctic sea ice [*Walsh and Chapman*, 2001; *Stroeve et al.*, 2005] and is suggestive of a common cause.

[21] Although we have noted the strong clustering of events, locally there is still scatter in event locations. Establishing whether events occur throughout the glacier (real scatter) or whether events occur at one location (scatter due to measurement) would give an important constraint on the physical mechanism of glacial earthquakes. Only regions K and H have enough events to make statistical statements about the local spatial distribution of events. In both regions, we find a distribution elongated in the direction of motion (see Figures 5b and 5c). In "sliding direction" coordinates, with x in the sliding direction and y perpendicular to the sliding direction, both regions have Gaussian distributions in x and y but with different standard deviations (σ_x and σ_y). For region K, σ_x = 10.4 km and σ_y = 7.0 km. For region H, σ_x = 10.9 km and σ_y = 7.4 km. For comparison, the region of H with surface velocities greater than 7 km/yr is approximately 10 km by 5 km (in x and y, respectively) [*Howat et al.*, 2005]. All other regions also have a larger scatter in the sliding direction, although we cannot make a statistical comparison due to insufficient data. We do not observe any pervasive preferential scatter in location that could be attributed to station coverage. Because of radiation patterns, locations should be slightly

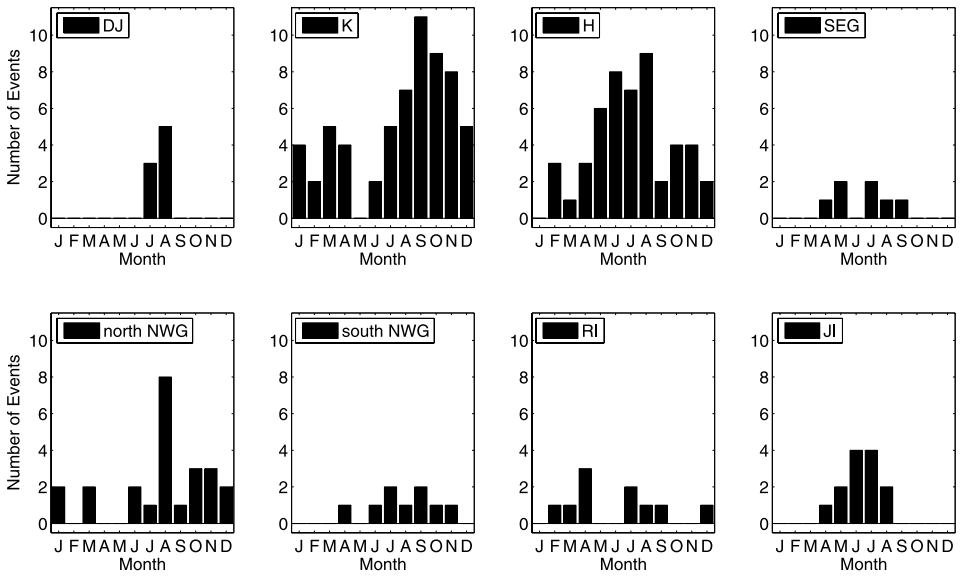

Figure 8. Regional monthly histograms for (top) east Greenland and (bottom) west Greenland over the time period 1993–2005. Region names are as in Figure 3.

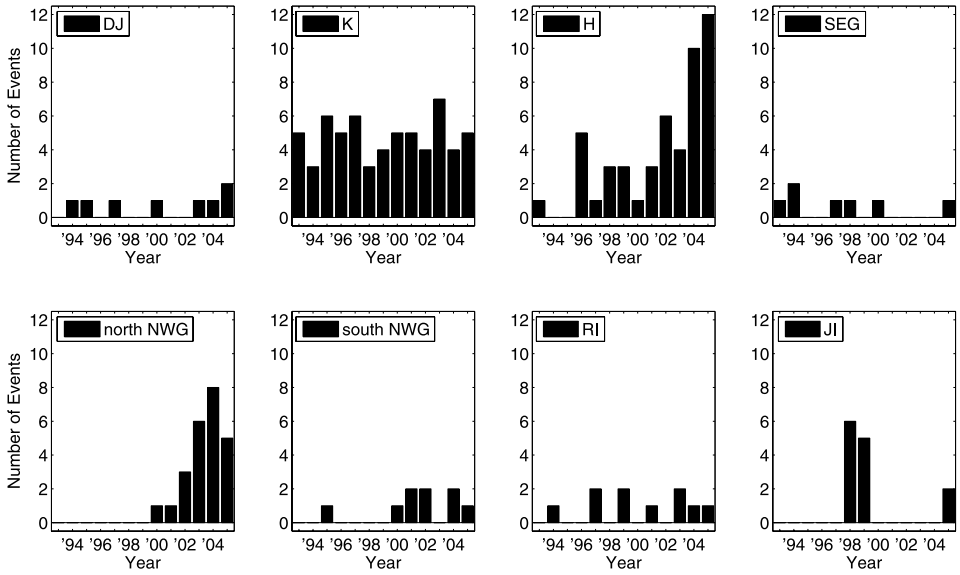

Figure 9. Regional yearly histograms for (top) east Greenland and (bottom) west Greenland. Region abbreviations are as in Figure 3.

better constrained in the sliding direction. Since we observe the opposite trend, the scatter in the sliding direction is likely real and not due to location errors. This has two possible implications. One possibility is that only a fraction of the whole glacier participates in individual glacial earthquakes. The scatter in locations should then be interpreted as due to sliding of different segments of the glacier. The other possibility is that the resistive force drops in a very heterogeneous fashion. Under this scenario, the scatter in locations should be interpreted as due to the drop in resistive force occurring primarily in different segments of the glacier in different events. With the data set considered here, the two scenarios are indistinguishable.

[22] Figure 10a shows the size distribution for all of the events. All events have amplitudes between $0.1-2.0 \times 10^{14}$ kg m. This corresponds to 100 km^3 of ice that travels a distance of 0.1–2.0 m (in roughly 50 s), although only the product of mass and distance is constrained. Using (1), (2) and (5), we can determine upper and lower bounds on the distance, velocity change, and change in average friction coefficient associated with each event. Taking 200 km^3 as an estimate of the size of the fast moving portion of the largest glacier, then $M = 2 \times 10^{14}$ kg and the lower bounds are $D =$ 0.2 meters, $V = 0.008$ m/s, and $\Delta f = 3 \times 10^{-5}$ for a typical event (0.4×10^{14} kg m). Taking $D = 100$ meters as an estimate for extreme values of slip, then $V = 4$ m/s, and $\Delta f =$ 0.016. Although it is unlikely that the average friction coefficient describes a physical coefficient of friction (i.e., the ratio of shear stress to normal stress), $\Delta f \cdot Mg$ can be thought of as the effective driving force so Δf still gives a useful constraint on the relative size of the effective driving force. It is difficult to compare such estimates of mass and velocity changes with those measured by more standard glaciological methods since temporal and spatial resolutions are typically quite different. However, the lower bound on velocity variations is higher than all other observed velocity variations [e.g., *Zwally et al.*, 2002; *Bindschadler et al.*, 2003] by at least a factor of 20. On the other hand, masses on the order of 100 km^3 have been observed to move coherently [e.g., *Joughin et al.*, 2004; *Luckman and Murray*, 2005] but have not previously been observed to do so on such short timescales.

[23] The scarcity of events with amplitudes below 0.3×10^{14} kg m may be a result of many events being just below the detection threshold and therefore not being counted. Fitting the remainder of the data to a line in log-log space yields a slope of -2.5. The slope deviates significantly from the classic Gutenberg-Richter relation (slope of -0.67). Furthermore, the data are not well fit by the best fit line. The reason for this poor fit becomes clear when one compares the size distributions of different regions. As shown in Figure 10b, the events in region K are larger on average and span a wider range of amplitudes as compared to events in region H which are smaller and have a narrower distribution of amplitudes. Only regions K and H have enough events to make a clear comparison, but the size distributions in all other regions are more similar to region H than region K. In fact, comparing Figure 10a with Figure 10b, we see that every event with amplitude greater than 0.9×10^{14} kg m occurs in region K.

[24] The distribution of events in region K provides additional constraints on the nature of glacial earthquakes. As stated above, the detection threshold is approximately 0.3×10^{14} kg m. We expect the threshold to be similar in all regions, yet region K has its peak number of events at 0.6×10^{14} kg m and contains fewer events with amplitudes between 0.3 and 0.5×10^{14} kg m. This implies that the distribution in region K is close to the true distribution of glacial earthquakes there, and not a result of the detection threshold. The lack of small events suggests the possibility that glacial earthquakes of a characteristic size are preferentially generated at each outlet glacier. If glacial earthquakes have such a characteristic size, then it would likely depends on a number of factors such as glacier size, hydrologic conditions and calving rate, some of which

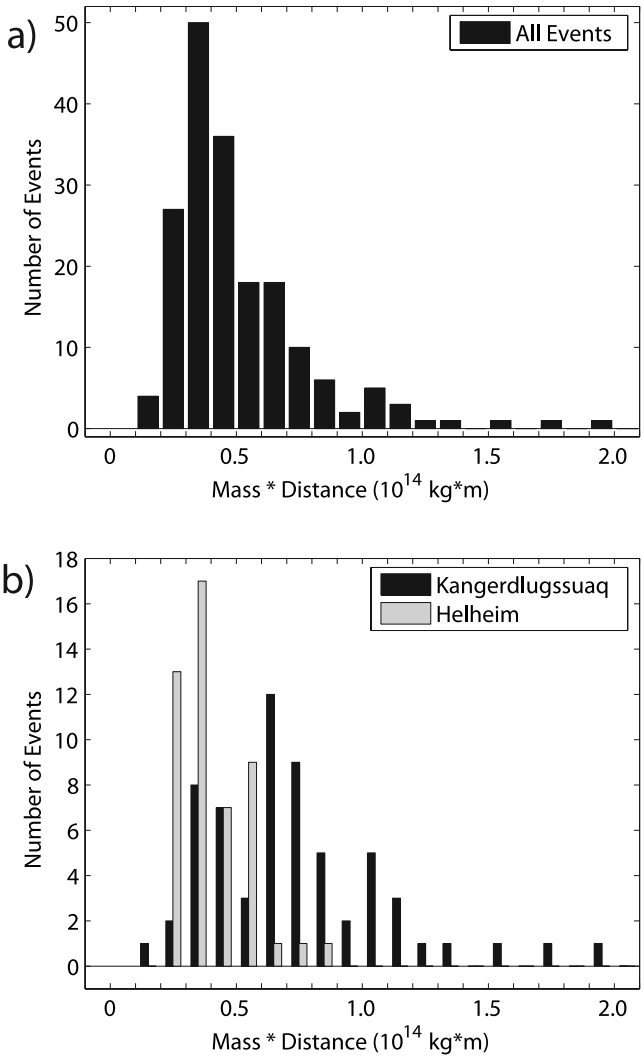

Figure 10. (a) Size distribution for all events. (b) Size distribution for regions K and H.

may change over time, and a power law distribution should not be expected, at least not locally.

5. Conclusions and Implications

[25] All 184 observed Greenland glacial earthquakes occur south of 78°N and in regions with ice flow velocities greater than 800 m/yr (ice streams and large outlet glaciers). All events have amplitudes between 0.1 and 2.0 $\times$ 10^{14} kg m. Events of smaller amplitude may exist but are not detected. All mechanisms are consistent with sliding of large masses of ice in the direction of glacial flow over a period of about 50 s, although additional observations are required to determine the degree to which this model is just an approximation of the actual source mechanism. The seasonality and increase in total number of events in the past few years suggests that glacial earthquakes are sensitive to temperature or variables affected by temperature. Although events are tightly clustered, locations have a wider spread in the sliding direction implying that events are not all colocated.

[26] Different glaciers display different glacial earthquake behavior. Each glacier has slightly different seasonal behavior, with peaks in activity in different months. Some glaciers but not all show the dramatic increase in number of events in the past few years. Some regions (e.g., region K) are consistent with a constant number of events per year whereas other regions (e.g., region NWG) have had an unmistakable dramatic increase during the same time period. Glacial earthquakes in region K are larger on average than in any other region, with these events comprising all of the events larger than 0.9 $\times$ 10^{14} kg m. The distribution of these (region K) events does not resemble a Gutenberg-Richter distribution, but instead has a peak at 0.6 $\times$ 10^{14} kg m, suggesting that glacial earthquakes may have a characteristic size that depends on attributes of the glacier where they occur.

[27] Any physical mechanism invoked to explain glacial earthquakes must satisfy the observational constraints presented here. Such a physical mechanism will necessarily change the understanding of glacial dynamics since glacial earthquakes are not predicted by any existing theory of glacial behavior. An improved understanding of glacial dynamics is needed to understand fully the stability of the Greenland ice sheet.

[28] **Acknowledgments.** We thank R. Anderson, T. Murray, S. Anandakrishnan, and an anonymous reviewer for helpful comments. This research was supported by a National Science Foundation Graduate Fellowship (VCT) and National Science Foundation grants EAR-0207608 and OPP-0352276. The seismic data were collected and distributed by the Incorporated Research Institutions for Seismology and the U.S. Geological Survey.

References

Alley, R. B., and I. M. Whillans (1991), Changes in the West Antarctic Ice Sheet, *Science*, *254*, 959–963.

Bamber, J. L., R. L. Layberry, and S. P. Gogineni (2001), A new ice thickness and bed data set for the Greenland ice sheet, *J. Geophys. Res.*, *106*, 33,773–33,780.

Bauer, A. (1961), Influence de la dynamique des fleuves de glace sur celle de l'Islandsis du Groenland, *Int. Assoc. Sci. Hydrol. Publ.*, *54*, 578–584.

Bindschadler, R. A., M. A. King, R. B. Alley, S. Anandakrishnan, and L. Padman (2003), Tidally controlled stick-slip discharge of a West Antarctic ice stream, *Science*, *301*, 1087–1089.

Brodsky, E. E., E. Gordeev, and H. Kanamori (2003), Landslide basal friction as measured by seismic waves, *Geophys. Res. Lett.*, *30*(24), 2236, doi:10.1029/2003GL018485.

Cappelen, J., B. V. Jorgensen, E. V. Laursen, L. S. Stannius, and R. S. Thomsen (2001), *Tech. Rep. 00-18*, Dan. Meteorol. Inst., Copenhagen.

Deichmann, N., J. Ansorge, F. Scherbaum, A. Aschwanden, F. Bernardi, and G. H. Gudmundsson (2000), Evidence for deep icequakes in an Alpine glacier, *Ann. Glaciol.*, *31*, 85–90.

Dziewonski, A. M., and D. L. Anderson (1981), Preliminary reference Earth model, *Phys. Earth Planet. Inter.*, *25*, 297–356.

Dziewonski, A. M., T. A. Chou, and J. H. Woodhouse (1981), Determination of earthquake source parameters from waveform data for studies of global and regional seismicity, *J. Geophys. Res.*, *86*, 2825–2852.

Ekström, G. (2006), Global detection and location of seismic sources by using surface waves, *Bull. Seismol. Soc. Am.*, *96*, 1201–1212.

Ekström, G., M. Nettles, and G. A. Abers (2003), Glacial earthquakes, *Science*, *302*, 622–624.

Ekström, G., A. M. Dziewonski, N. N. Maternovskaya, and M. Nettles (2005), Global seismicity of 2003: Centroid-moment-tensor solutions for 1087 earthquakes, *Phys. Earth Planet. Inter.*, *148*, 327–351.

Ekström, G., M. Nettles, and V. C. Tsai (2006), Seasonality and increasing frequency of Greenland glacial earthquakes, *Science*, *311*, 1756–1758, doi:10.1126/science.1122112.

Hooke, R. L. (2005), *Principles of Glacier Mechanics*, 2nd ed., Cambridge Univ. Press, New York.

Howat, I. M., I. Joughin, S. Tulaczyk, and S. Gogineni (2005), Rapid retreat and acceleration of Helheim Glacier, east Greenland, *Geophys. Res. Lett.*, *32*, L22502, doi:10.1029/2005GL024737.

Joughin, I., W. Abdalati, and M. Fahnestock (2004), Large fluctuations in speed on Greenland's Jakobshavn Isbrae glacier, *Nature*, *432*, 608–610.

Kanamori, H., and J. W. Given (1982), Analysis of long-period seismic waves excited by the May 18, 1980, eruption of Mount St. Helens: A terrestrial monopole, *J. Geophys. Res.*, *87*, 5422–5432.

Kawakatsu, H. (1989), Centroid single force inversion of seismic waves generated by landslides, *J. Geophys. Res.*, *94*, 12,363–12,374.

Luckman, A., and T. Murray (2005), Seasonal variation in velocity before retreat of Jakobshavn Isbrae, Greenland, *Geophys. Res. Lett.*, *32*, L08501, doi:10.1029/2005GL022519.

Morgan, V. I., T. H. Jacka, G. J. Akerman, and A. L. Clarke (1982), Outlet glacier and mass-budget studies in Enderby, Kemp, and MacRobertson Lands, Antarctica, *Ann. Glaciol.*, *3*, 204–210.

Paterson, W. S. B. (2002), *The Physics of Glaciers*, 3rd ed., Elsevier, New York.

Qamar, A. (1988), Calving icebergs: A source of low-frequency seismic signals from Columbia Glacier, Alaska, *J. Geophys. Res.*, *93*, 6615–6623.

Rignot, E., D. Braaten, S. P. Gogineni, W. B. Krabill, and J. R. McConnell (2004), Rapid ice discharge from southeast Greenland glaciers, *Geophys. Res. Lett.*, *31*, L10401, doi:10.1029/2004GL019474.

Smith, G. P., and G. Ekström (1997), Interpretation of earthquake epicenter and CMT centroid locations in terms of rupture length and direction, *Phys. Earth Planet. Inter.*, *102*, 123–132.

Stroeve, J. C., M. C. Serreze, F. Fetterer, T. Arbetter, W. Meier, J. Maslanik, and K. Knowles (2005), Tracking the Arctic's shrinking ice cover: Another extreme September minimum in 2004, *Geophys. Res. Lett.*, *32*, L04501, doi:10.1029/2004GL021810.

Stuart, G., T. Murray, A. Brisbourne, P. Styles, and S. Toon (2005), Seismic emissions from a surging glacier: Bakaninbreen, Svalbard, *Ann. Glaciol.*, *42*, 151–157.

Van Wormer, D., and E. Berg (1973), Seismic evidence for glacier motion, *J. Glaciol.*, *12*, 259–265.

Walsh, J. E., and W. L. Chapman (2001), 20th-century sea-ice variations from observational data, *Ann. Glaciol.*, *33*, 444–448.

Weaver, C. S., and S. D. Malone (1979), Seismic evidence for discrete glacier motion at the rock-ice interface, *J. Glaciol.*, *23*, 171–184.

Wolf, L. W., and J. N. Davies (1986), Glacier-generated earthquakes from Prince William Sound, Alaska, *Bull. Seismol. Soc. Am.*, *76*, 367–379.

Zwally, H. J., W. Abdalati, T. Herring, K. Larson, J. Saba, and K. Steffen (2002), Surface melt-induced acceleration of Greenland ice-sheet flow, *Science*, *297*, 218–222.

G. Ekström and V. C. Tsai, Department of Earth and Planetary Sciences, Harvard University, 20 Oxford Street, Cambridge, MA 02138, USA. (vtsai@fas.harvard.edu)